ScienceDirect

Contents lists available at ScienceDirect

Journal of Iron and Steel Research, International

journal homepage: www.chinamet.cn

Plasticity performance of $Al_{0.5}CoCrCuFeNi$ high-entropy alloys under nanoindentation

Li-ping Yu[1], Shu-ying Chen[2], Jing-li Ren[1,3,*], Yang Ren[4], Fu-qian Yang[5], Karin A. Dahmen[6], Peter K. Liaw[2,**]

[1] School of Mathematics and Statistics, Zhengzhou University, Zhengzhou 450001, Henan, China
[2] Department of Materials Science and Engineering, The University of Tennessee, Tennessee 37996, USA
[3] State Key Laboratory of Nonlinear Mechanics, Institute of Mechanics, CAS, Beijing 100190, China
[4] X-ray Science Division, Argonne National Laboratory, Illinois 60439, USA
[5] Department of Chemical and Materials Engineering, University of Kentucky, Kentucky 40506, USA
[6] Department of Physics, University of Illinois at Urbana-Champaign, Illinois 61801, USA

ARTICLE INFO

Key words:
High-entropy alloys
Nanoindentation
Critical behavior
Chaotic behavior

ABSTRACT

The statistical and dynamic behaviors of the displacement-load curves of a high-entropy alloy, $Al_{0.5}CoCrCuFeNi$, were analyzed for the nanoindentation performed at two temperatures. Critical behavior of serrations at room temperature and chaotic flows at 200 ℃ were detected. These results are attributed to the interaction among a large number of slip bands. For the nanoindentation at room temperature, recurrent partial events between slip bands introduce a hierarchy of length scales, leading to a critical state. For the nanoindentation at 200 ℃, there is no spatial interference between two slip bands, which is corresponding to the evolution of separated trajectory of chaotic behavior.

1. Introduction

Serrated flow, associated with cyclic softening and hardening of materials, during plastic deformation, has been studied extensively since the discovery of the Portevin-Le Chatelier (PLC) effect[1]. It is one of the few prominent examples of the complexity of the spatiotemporal dynamics arising from the collective behavior of defect populations[2]. The discontinuous serrated flow indicates that the material responds in a jerky way with stress drops, reflecting sudden-local softening in the material. Understanding the intriguing spatio-temporal instability and its influence on the mechanical properties of various materials has drawn great attentions, the results on nanometer-sized single crystals[3,4], microcrystals[5-7] and bulk metallic glasses[8-12] can be found.

As a new class of materials, high-entropy alloys (HEAs) found in 1990′s have been continuously studied[13-32]. For slow compression or tension at certain temperatures and (small) strain rates, HEAs deform via sudden slips that are associated with the stress drops in stress-strain curves[17-22]. Zhang et al.[17] pointed out that the serrations of HEAs during the compression tests at the strain rate of 10^{-3} s^{-1} seem to be greater than those at the strain rate of 10 s^{-1}. Carroll et al.[22] found that at a strain rate of 10^{-4} s^{-1}, the serrated stress-strain curves of the CoCrFeMnNi HEA move from type-A to B to C PLC-band with increasing temperature from 200 to 620 ℃. Recently, Chen et al.[23] first investigated the serration behavior of a high-entropy alloy $Al_{0.5}CoCrCuFeNi$ in nanoindentation test at holding time of 5, 10, and 20 s (when the load reaches the maximum value of 100 mN, then maintained at 100 mN for different time of 5, 10, and 20 s). They divided serrated flow into three stages: loading stage, holding stage and unloading stage; then they found the displacement sequence at holding stage manifests a chaotic behavior. Naturally, a new question arises: whether the dynamic behavior at loading stage is also chaotic or not and what is the underlying mechanism of the serrated flow at

L.P. Yu and S.Y. Chen are joint first authors.
* Corresponding author. Prof., Ph.D.
E-mail address: *renjl@zzu.edu.cn* (*J. L. Ren*).
** Corresponding author. Prof., Ph.D.
E-mail address: *pliaw@utk.edu* (*P. K. Liaw*).

Received 8 December 2016; Received in revised form 20 February 2017; Accepted 21 February 2017
Available online 15 April 2017

loading stage. Motivated by these, here nanoindentation was used to study the displacement burst at loading stage of the $Al_{0.5}$CoCrCuFeNi HEA at room temperatures and 200 ℃. The dynamical analysis and statistical analysis are conducted for plastic dynamics at two temperatures.

2. Experimental

The $Al_{0.5}$CoCrCuFeNi (molar ratio) HEA in the shape of cylindrical rod was fabricated by arc-melting the mixed principal elements with high purity (purity exceeding 99.9 wt.%) in a water-cooled copper mold. Repeated melting for at least five times was carried out to improve the homogeneity of the material. The molten alloy was drop-cast into copper molds with 2 mm in diameter. Disks cut from the as-cast $Al_{0.5}$CoCrCuFeNi HEA rods were mechanically ground and polished to obtain two parallel surfaces of a mirror quality to avoid surface effects.

The nanoindentation tests were carried out using a Nano Test Vantage (Micro Materials). A diamond Berkevich indenter with a nominal tip radius of about 50 nm was used. The machine compliance was calibrated to be 0.30 nm/mN. The nanoindentation test was performed under the mode of load control with the peak load of 100 mN. Both the loading rate and unloading rate were 10.00 mN/s. Indentation tests were performed at two temperatures (room temperature and 200 ℃). For each indentation condition, at least 3 indents were performed. The indentation depth and indentation load were used to analyze the near-surface mechanical behavior of the $Al_{0.5}$CoCrCuFeNi HEA.

3. Results and Discussion

Fig. 1(a) shows typical indentation load-displacement (σ-h) curves at different temperatures. The load-displacement curves seem to be regular in the loading stage, and there are no obvious shear steps. The amplification of the curves in the loading stages reveals the presence of the displacement-drop events, as shown in Fig. 1(b). It needs to eliminate the influence from the indentation depth increase in order to analyze these events[33]. A polynomial function ($y=A+B_1x+B_2x^2$) was used to establish a baseline by fitting the indentation displacement-load curves in the loading stage. Using the baseline, the variation of the normalized serration with the indentation load is inserted in Fig. 1(b).

The serrated flow presented in the indentations at room temperature and 200 ℃ can then be determined, as shown in Fig. 2(a). Introducing a variable

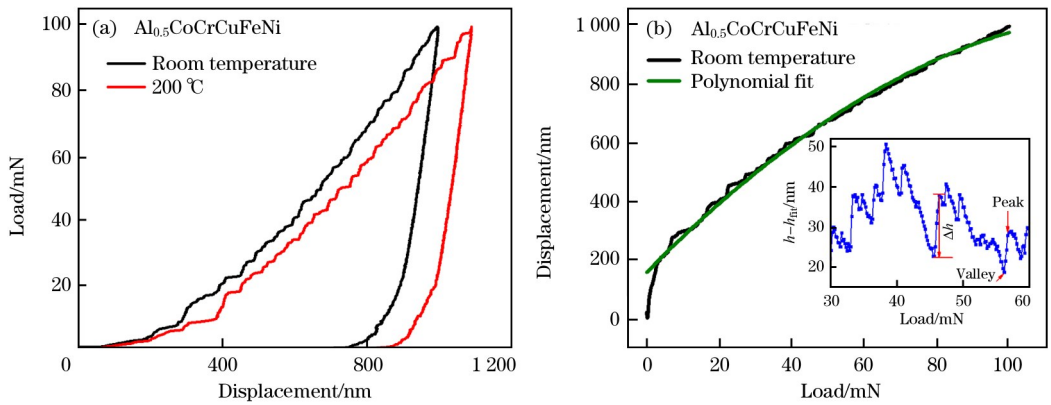

Fig. 1. Load-displacement curves during nanoindentation at room temperature and 200 ℃ of high-entropy alloy $Al_{0.5}$CoCrCuFeNi (a) and polynomial function fitting curve of displacement-load (the inset shows the serration events) (b).

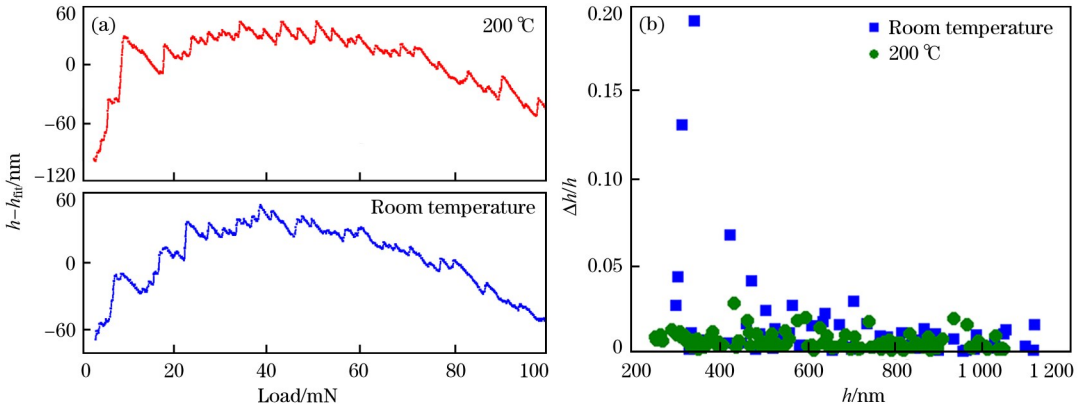

Fig. 2. Serration events on high-entropy alloy $Al_{0.5}$CoCrCuFeNi at room temperature and 200 ℃ (a) and displacement burst size distribution as a function of depth at two temperatures (b).

of Δh (the difference of the displacement between the maximum and previous minimum value was taken as displacement drop by Δh), one can generate the normalization, $S=\Delta h/h$ of the Δh value by the depth, h, which is carried out to eliminate the statistical error[34]. The variation of the displacement burst size with the indentation depth at room temperature and 200 ℃ is depicted in Fig. 2(b). The size distribution of the displacement bursts for the nanoindentation at room temperature seems to have a floating behavior with increasing indentation depth, while the size distribution of the displacement burst at 200 ℃ does not possess this obvious characteristic.

Load-time curves and depth-time curves during nanoindentation at room temperature and 200 ℃ of the high-entropy alloy $Al_{0.5}CoCrCuFeNi$ are shown in Fig. 3. A linear relationship in load-time curve whether it is in loading procedure or unloading procedure can be found. In Fig. 3(b, d), t_l represents accumulation time and t_r represents relaxation time. Average values of t_l and t_r in serrated flow at room temperature and 200 ℃ are listed in Table 1. It is obtained that compared with 200 ℃, average values of t_l and t_r at room temperature decrease. Further from Table 1, $t_l<t_r$ means that energy releasing exists in the deformation, and the release process is relatively

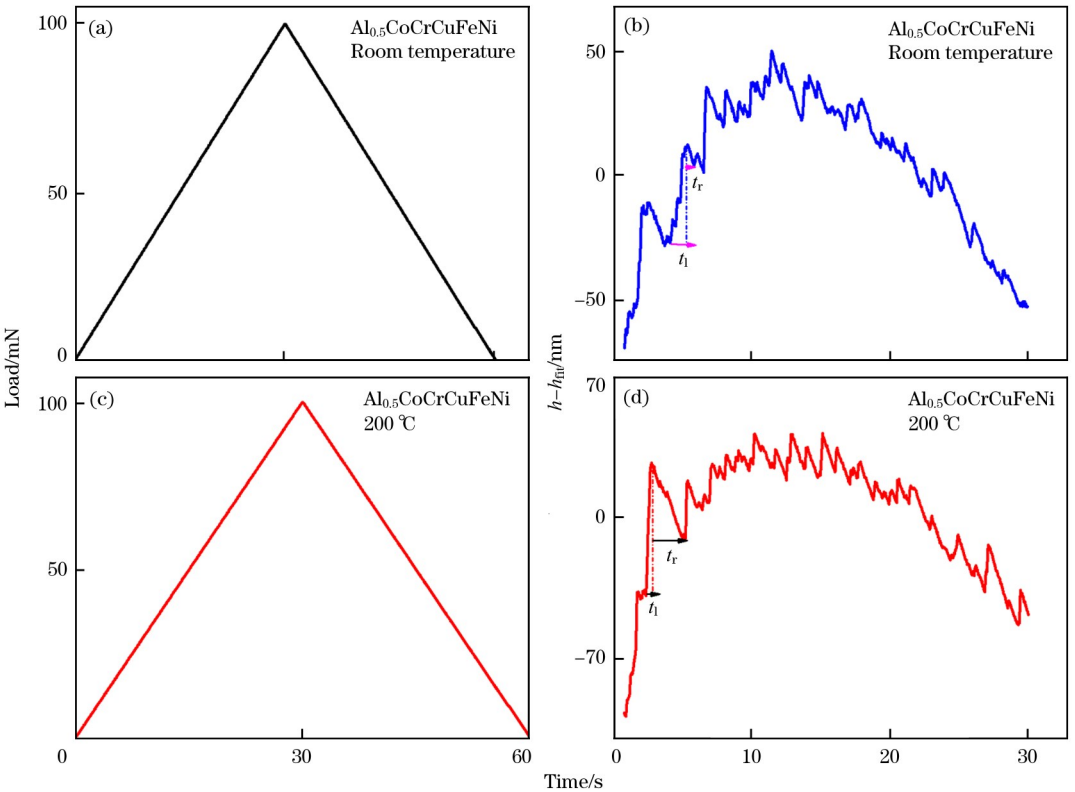

Fig. 3. Load-time curve (a, c) and depth-time curve (b, d) during nanoindentation at room temperature and 200 ℃ of high-entropy alloy $Al_{0.5}CoCrCuFeNi$.

Table 1
Dynamic parameters for nanoindentation at room temperature (RT) and 200 ℃

Temperature	t_l/s	t_r/s	τ	m	λ_1
RT	0.0866	0.1598	3	8	−0.0123
200 ℃	0.0941	0.2192	9	6	0.0123

Note: τ—Time delay; m—Embedding dimension; λ_1—Largest Lyapunov exponent.

slow at some time in serration events.

To reveal the information in the serration response of the $Al_{0.5}CoCrCuFeNi$ HEA at two temperatures, a dynamic analysis of the displacement sequence, $\{h(l), l=1,2,\cdots,N\}$, was performed. As described by Strogatz[35], an unknown chaotic, dynamical system has equivalent geometrical characteristics with the model in the reconstructed m-dimensional phase space. Thus, an original, chaotic dynamics can be studied through the reconstruction of the phase space. The reconstruction of a phase space for the displacement sequence of $\{h(l), l=1,2,\cdots,N\}$ can be performed as follows. Given a time series, $\{h(l), l=1,2,\cdots,N\}$, the mutual information method[36] was used to obtain a time-delay reconstruction of a phase space. The Cao-method[37] was employed for the computation of the embedding dimension. After selecting τ, and m, the time series, an m-dimensional vector of $\boldsymbol{Y}(t_i)=\{h(t_i), h(t_i+\tau), \cdots, h(t_i+(m-1)\tau), t_i=1,\cdots,[N-(m-1)\tau]\}$ was constructed from the sequence, $\{h(l), l=1,2,\cdots,$

N}. The Eckmann's algorithm[38] was used to find the largest Lyapunov exponent with the selected delay and embedding dimension. Firstly, one takes an initial point, $\boldsymbol{Y}(t_1)$ and its nearest neighbor point, $\boldsymbol{Y}_1(t_1)$ (according to the Euclidian module in the reconstructed phase space), and denotes $\boldsymbol{L}_1=\boldsymbol{Y}(t_1)-\boldsymbol{Y}_1(t_1)$. After an iteration time, the points, $\boldsymbol{Y}(t_1)$ and $\boldsymbol{Y}_1(t_1)$, transform into $\boldsymbol{Y}(t_2)$ and $\boldsymbol{Y}_2(t_2)$ with $\boldsymbol{L}_2=\boldsymbol{Y}(t_2)-\boldsymbol{Y}_2(t_2)$. According to the least-squares method, there is a matrix, $\boldsymbol{T}_1$, which maps the evolution from $\boldsymbol{L}_1$ to $\boldsymbol{L}_2$, i. e., $\boldsymbol{L}_2=\boldsymbol{T}_1\boldsymbol{L}_1$. Repeating the above steps from $\boldsymbol{Y}(t_i)$ to $\boldsymbol{Y}(t_{i+1})$, a series of $\boldsymbol{T}_i(i=1,2,\cdots,p)$ can be obtained. Using the standard $\boldsymbol{QR}$ decomposition ($\boldsymbol{Q}$ is an orthogonal matrix, and $\boldsymbol{R}$ is an upper triangle matrix with positive diagonal elements) for the matrix, $\boldsymbol{T}_i$, where $\boldsymbol{T}_i=\boldsymbol{Q}_i\boldsymbol{R}_i$, the Lyapunov exponents are calculated as $\lambda_k=1/(t_p-t_1)\sum_{j=1}^{p}\ln(R_j)_{kk}$, $k=1,2,\cdots,m$ (t_1 and t_p are initial and final time, respectively).

Note that the Lyapunov exponent of the dynamic system is associated with the corresponding dynamic behavior. For the largest Lyapunov exponent being negative, the two adjacent orbits in the dynamical system will be convergent to a stable state. For the largest Lyapunov exponent being positive, these two orbits will be separated finally, which corresponds to a chaotic behavior. The largest Lyapunov exponents for the displacement sequence, observed during the indentation at two temperatures, are listed in Table 1. The largest Lyapunov exponents vary from a negative value at room temperature to a positive value at 200 ℃.

Using the method proposed by Grassberger and Procaccia[39], named the G-P algorithm, one can calculate the correlation dimension associated with the correlations among points of time series on the chaotic attractor. A positive Lyapunov exponent and a finite correlation dimension are two criteria for determining chaos. The greater the value of positive Lyapunov exponent, the faster the speed of adjacent orbits divergence. The greater the value of correlation dimension, the more meticulous the structure of attractor. Further these two methods are more effective for dense time sequences. Next the correlation dimension is calculated to further verify the chaotic behavior.

Given a signal, $\{h(l),l=1,2,\cdots,N\}$, of points obtained from the displacement sequence, with $h_i=h(t+i\delta)$, where δ is a fixed time increment, one can use the standard technique of delay coordinate embedding[40] to reconstruct a state space, with an appropriate choice of the delay time[41] and a d-dimensional phase space[42]. Due to the divergence of trajectories, most pairs, (h_i, h_j), with $i\neq j$ will be dynamically uncorrelated, while the points lying on the attractor will be spatially correlated. The definition of the correlation integral is $C(r)=1/N\sum_{i,j=1}^{N}\Theta(x)(r-|h_i-h_j|)$, where $\Theta(x)$ is the Heaviside function (Heaviside(x) returns the value, 0 for $x<0$, 1 for $x>0$, and 1/2 for $x=0$), r is the radius of the Heaviside function, and N is the number of points. For a self-similar chaotic attractor, there is the following relation: $C(r)\sim r^{\nu}$ in the limit of small r, where ν is the correlation dimension. For a low-dimensional dynamical system, the slope in the plot of $\ln C(r)$ versus $\ln r$ increases with the embedding dimension, d, until it reaches a plateau; its value at the plateau is, then, taken as the estimate of the correlation dimension[39,43]. That is to say, as d is increased, the slope in the plot of $\ln C(r)$ versus $\ln r$ has a convergence for chaotic behavior[44].

Fig. 4 depicts the plots of $\ln C(r)$ versus $\ln r$ for the nanoindentation at 200 ℃ and room temperature with the embedding dimension of $d=6-9$ and $d=6-10$, respectively. It is evident that the slopes are converged with decreasing r at 200 ℃ (Fig. 4(a)), and

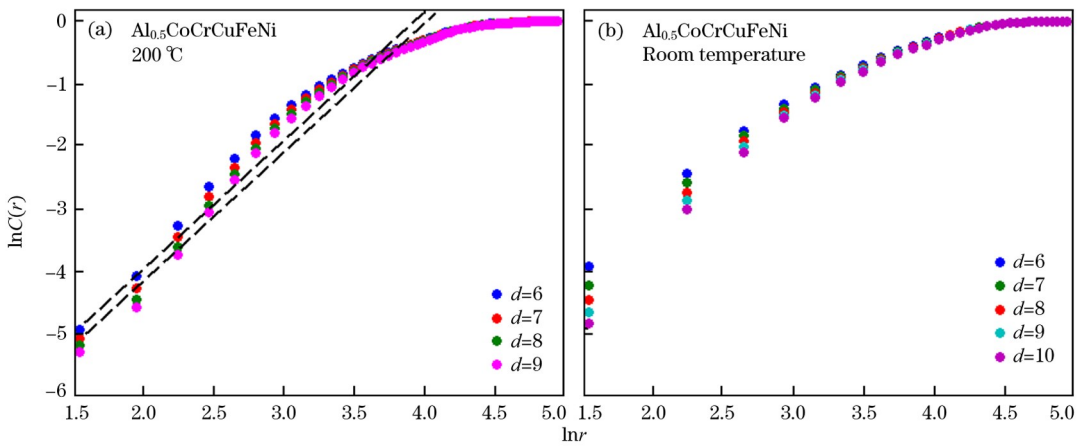

Fig. 4. Log-log plot of correlation integral as a function of r of displacement-load for high-entropy alloy $Al_{0.5}CoCrCuFeNi$ at 200 ℃ for $d=6-9$ with the delay of 9 (a) and room temperature for $d=6-10$ with the delay of 3 (b).

there is no convergence of the slopes with decreasing r at room temperature (Fig. 4(b)). One can calculate the converged value of the slopes of $\ln C(r)$ of the displacement signal: the correlation dimension, $\nu \approx 1.24$. Thus, it also allows one to conclude the existence of chaotic behavior for the displacement sequence at 200 ℃[38,39,44].

The self-similarity of chaotic attractor can be confirmed by correlation dimension. A large correlation dimension suggests the concurrent nucleation of a large number of slip bands throughout the material. The higher density of slip bands in turn can induce a hierarchical structure of slip bands[11]. Then, the slip bands have a self-similar structure due to the interactions among the hierarchies of slip bands at different positions and in different directions.

Senkov et al.[19] showed that dislocation motion is highly sensitive to temperature, and the critical resolved shear stress for dislocation gliding decreases rapidly with increasing temperature. It indicates that an elevated temperature allows atoms to have more chance to successfully lock dislocations, and then, have enough time to relax elastic energy, which indicates a lack of internal energy for the formation of new slip bands. In addition, the relaxation time is relatively large at 200 ℃ (Table 1). There is no spatial interference between two slip bands, which will be separated under the time evolution. The evolution of the separated trajectory is corresponding to the chaotic behavior.

For the nanoindentation at room temperature, the non-convergence of $\ln C(r)$ and negative largest Lyapunov exponent suggest no evidence of chaotic dynamic. To further explore the dynamical behavior of the nanoindentation of the $Al_{0.5}CoCrCuFeNi$ HEA, a statistical analysis of displacement-load curves at two temperatures is carried out. The load interval between a displacement minimum and the subsequent maximum values was used to represent the duration of the load drop, which is denoted by $\Delta\sigma$. The distribution, $D(\Delta h)$, of Δh was investigated for the indentations at room temperature and 200 ℃. Similarly, the distribution, $D(\Delta\sigma)$, of the corresponding $\Delta\sigma$ was also studied. Figs. 5 and 6 show the plots of $D(\Delta h)$ and $D(\Delta\sigma)$ at room temperature and 200 ℃, respectively. There is a peaked distribution of $D(\Delta\sigma)$ in Fig. 6(b), which indicates no existence of a power-law distribution. It is evident that the distributions of $D(\Delta h)$ and $D(\Delta\sigma)$ at room temperature have the form of $D(\Delta h) \sim \Delta h^{-\beta}$ with $\beta = 1.68$ and $D(\Delta\sigma) \sim \Delta\sigma^{-\alpha}$ with $\alpha = 1.50$. Furthermore, it is found that the conditional average of $<\Delta h> \sim \Delta\sigma^{-x}$ with $x = 0.74$ (Fig. 5(c)). Thus, the scaling relation of $\alpha = x(\beta - 1) + 1$[45] is satisfied, which characterizes a critical be-

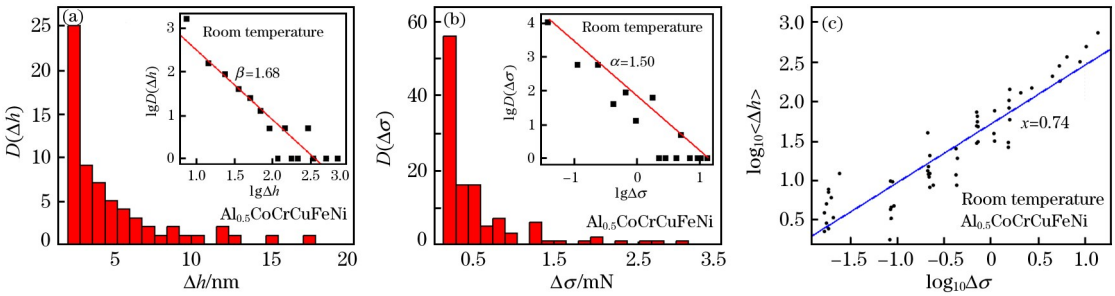

Fig. 5. Distributions of displacement drop (a) and load duration (b) for high-entropy alloy $Al_{0.5}CoCrCuFeNi$ at room temperature and conditional average of displacement drops as a function of size of load duration for high-entropy alloy $Al_{0.5}CoCrCuFeNi$ at room temperature (c).

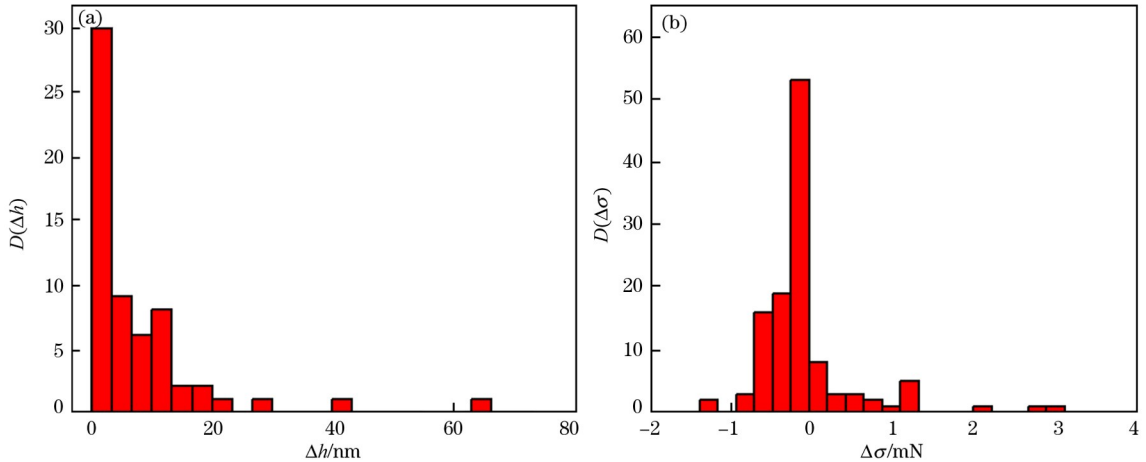

Fig. 6. Distributions of displacement drops (a) and load duration (b) for high-entropy alloy $Al_{0.5}CoCrCuFeNi$ at 200 ℃.

havior and an order state. This result is interpreted that the dislocation motion is accompanied with the increase of the mutual interference of slip bands at room temperature, which results in criticality and plastic deformation.

4. Summary

A plastic dynamic behavior for the nanoindentation of the $Al_{0.5}CoCrCuFeNi$ HEA is observed from the statistical and dynamical analyses. The chaotic behavior characterized by a positive Lyapunov exponent for the displacement series, $\{h(l), l=1,2,\cdots, N\}$, occurs at 200 ℃. The criticality, characterized by the intermittent power-law distribution of the displacement drops, is observed at room temperature. The relaxation time decreases with decreasing temperature. Thus, for the nanoindentation at room temperature, there is no enough time to release elastic energy, and there is the formation of new slip bands adjacent to existent bands in the region with the unreleased elastic energy. The overlaps of recurrent slip bands forming result in a hierarchy, leading to the critical state of the displacement-load series and plastic deformation. For the nanoindentation at elevated temperatures, there is enough time to release elastic energy, and these orbits will be separated finally, which is corresponding to chaotic behavior.

Acknowledgment

This work is supported by grants from the NSFC (11271339), the Plan for Scientific Innovation Talent of Henan Province (164200510011) and Innovative Research Team of Science and Technology in Henan Province (17IRTSTHN007), Opening Fund of State Key Laboratory of Nonlinear Mechanics, the US National Science Foundation (CMMI1100080 and DMR-1611180), the US department of Energy (DPE), Office of Fossil Energy, National Energy Technology Laboratory (Grant No. DE-FE-0008855, DE-FE-0011194, and DE-FE0024054), and the US Army Research Office (Grant No. W911NF-13-1-0438).

References

[1] A. Portevin, F. Le Chatelier, C. R. Acad. Sci. Paris. 176 (1923) 507-510.
[2] M. S. Bharathi, M. Lebyodkin, G. Ananthakrishna, C. Fressengeas, L. P. Kubin, Phys. Rev. Lett. 87 (2001) 165508.
[3] K. A. Dahmen, Y. Ben-Zion, J. T. Uhl, Phys. Rev. Lett. 102 (2009) 175501.
[4] N. Friedman, A. T. Jennings, G. Tsekenis, J. Y. Kim, M. Tao, J. T. Uhl, J. R. Greer, K. A. Dahmen, Phys. Rev. Lett. 109 (2012) 095507.
[5] M. C. Miguel, A. Vespignani, S. Zapperi, J. Weiss, J. R. Grasso, Nature 410 (2001) 667-671.
[6] M. Koslowski, R. LeSar, R. Thomson, Phys. Rev. Lett. 93 (2004) 125502.
[7] J. Weiss, D. Marsan, Science 299 (2003) 89-92.
[8] J. L. Ren, C. Chen, G. Wang, N. Mattern, J. Eckert, AIP Adv. 1 (2011) 032158.
[9] J. L. Ren, C. Chen, Z. Y. Liu, R. Li, G. Wang, Phys. Rev. B 86 (2012) 134303.
[10] J. L. Ren, C. Chen, G. Wang, W. S. Cheung, B. A. Sun, N. Mattern, S. Siegmund, J. Eckert, J. Appl. Phys. 116 (2014) 033520.
[11] C. Chen, J. L. Ren, G. Wang, K. A. Dahmen, P. K. Liaw, Phys. Rev. E 92 (2015) 012113.
[12] J. W. Qiao, Y. Zhang, J. Iron Steel Res. Int. 23 (2016) 7-13.
[13] J. W. Yeh, S. K. Chen, S. J. Lin, J. Y. Gan, T. S. Chin, T. T. Shun, C. H. Tsau, S. Y. Chang, Adv. Eng. Mater. 6 (2004) 299-303.
[14] B. Cantor, I. T. H. Chang, P. Knight, A. J. B. Vincent, Mater. Sci. Eng. A 375 (2004) 213-218.
[15] Y. Zhang, Y. J. Zhou, J. P. Lin, G. L. Chen, P. K. Liaw, Adv. Eng. Mater. 10 (2008) 534-538.
[16] B. Gludovatz, A. Hohenwarter, D. Catoor, E. H. Chang, E. P. George, R. O. Ritchie, Science 345 (2014) 1153-1158.
[17] Y. Zhang, T. T. Zuo, Z. Tang, M. C. Gao, K. A. Dahmen, P. K. Liaw, Z. P. Lu, Prog. Mater. Sci. 61 (2014) 1-93.
[18] J. W. Qiao, S. G. Ma, E. W. Huang, C. P. Chuang, P. K. Liaw, Y. Zhang, Mater. Sci. Forum 688 (2011) 419-425.
[19] O. N. Senkov, J. M. Scott, S. V. Senkova, D. B. Miraclea, C. F. Woodward, J. Mater. Sci. 47 (2012) 4062-4074.
[20] C. J. Tong, M. R. Chen, S. K. Chen, J. W. Yeh, T. T. Shun, S. J. Lin, S. Y. Chang, Metall. Mater. Trans. A 36 (2005) 1263-1271.
[21] J. Antonaglia, X. Xie, Z. Tang, C. W. Tsai, J. W. Qiao, Y. Zhang, M. O. Laktionova, E. D. Tabachnikova, J. W. Yeh, O. N. Senkov, JOM 66 (2014) 2002-2008.
[22] R. Carroll, C. Lee, C. W. Tsai, J. W. Yeh, J. Antonaglia, B. A. W. Brinkman, M. LeBanc, X. Xie, S. Y. Chen, P. K. Liaw, K. A. Dahmen, Sci. Rep. 5 (2015) 16997.
[23] S. Y. Chen, L. P. Yu, J. L. Ren, X. Xie, X. P. Li, Y. Xu, G. F. Zhao, P. Z. Li, F. Q. Yang, Y. Ren, P. K. Liaw, Sci. Rep. 6 (2016) 29798.
[24] M. C. Gao, J. W. Yeh, P. K. Liaw, Y. Zhang, High-Entropy Alloys: Fundamentals and Applications, Springer, Cham, Switzerland, 2016.
[25] M. A. Hemphill, T. Yuan, G. Y. Wang, J. W. Yeh, C. W. Tsai, A. Chuang, P. K. Liaw, Acta Mater. 60 (2012) 5723-5734.
[26] O. N. Senkov, G. B. Wilks, D. B. Miracle, C. P. Chuang, P. K. Liaw, Intermetallics 18 (2010) 1758-1765.
[27] Z. Tang, T. Yuan, C. W. Tsai, J. W. Yeh, C. D. Lundin, P. K. Liaw, Acta Mater. 99 (2015) 247-258.
[28] M. Seifi, D. Li, Z. Yong, P. K. Liaw, J. J. Lewandowski, JOM 67 (2015) 2288-2295.
[29] L. J. Santodonato, Y. Zhang, M. Feygenson, C. M. Parish, M. C. Gao, R. J. K. Weber, J. C. Neuefeind, Z. Tang, P. K. Liaw, Nat. Commun. 6 (2015) 5964.
[30] S. Q. Xia, Z. Wang, T. F. Yang, Y. Zhang, J. Iron Steel Res. Int. 22 (2015) 879-884.
[31] X. T. Liu, W. B. Lei, Q. J. Wang, W. P. Tong, C. S. Liu, J. Z. Cui, J. Iron Steel Res. Int. 23 (2016) 1195-1199.
[32] Y. Zhang, J. W. Qiao, P. K. Liaw, J. Iron Steel Res. Int. 23 (2016) 2-6.
[33] X. L. Bian, G. Wang, K. C. Chan, J. L. Ren, Y. L. Gao, Q. J. Zhai, Appl. Phys. Lett. 103 (2013) 101907.
[34] B. A. Sun, H. B. Yu, W. Jiao, H. Y. Bai, D. Q. Zhao, W. H. Wang, Phys. Rev. Lett. 105 (2010) 035501.
[35] S. H. Strogatz, Nonlinear Dynamics and Chaos, MA: Perseus Books, Cambridge, 1994.
[36] A. M. Fraser, H. L. Swinney, Phys. Rev. A 33 (1986) 1134-1140.
[37] L. Y. Cao, Physica D: Nonlinear Phenomena 110 (1997) 43-50.
[38] J. P. Eckmann, S. O. Kamphorst, D. Ruelle, S. Ciliberto, Phys. Rev. A 34 (1986) 4971-4979.
[39] P. Grassberger, I. Procaccia, Phys. Rev. Lett. 50 (1983) 346-349.

[40] D. A. Rand, L. S. Young, Dynamical Systems and Turbulence, Springer-Verlag, Berlin, 1981.
[41] H. Kantz, T. Schreiber, Nonlinear Time Series Analysis, Cambridge University Press, Cambridge, 1997.
[42] J. Theiler, Phys. Rev. A 34 (1986) 2427-2432.
[43] M. Ding, C. Grebogi, E. Ott, T. Sauer, J. A. Yorke, Phys. Rev. Lett. 70 (1993) 3872-3875.
[44] R. Sarmah, G. Ananthakrishna, B. A. Sun, W. H. Wang, Acta Mater. 59 (2011) 4482-4493.
[45] I. Råfols, E. Vives, Phys. Rev. B 52 (1995) 12651-12656.